Electrical Impedance Tomography: 3D Reconstructions using Scattering Transforms

Delbary, Fabrice; Hansen, Per Christian; Knudsen, Kim

Published in:
Applicable Analysis

Link to article, DOI:
10.1080/00036811.2011.598863

Publication date:
2012

Document Version
Early version, also known as pre-print

Electrical Impedance Tomography: 3D Reconstructions using Scattering Transforms

Fabrice Delbary,[a] Per Christian Hansen[a] and Kim Knudsen[b*]

[a] *Department of Informatics and Mathematical Modelling, Richard Petersens Plads, Building 321, Technical University of Denmark, DK-2800 Kgs. Lyngby, Denmark*
[b] *Department of Mathematics, Matematiktorvet, Building 303S, Technical University of Denmark, DK-2800 Kgs. Lyngby, Denmark*

(*June 2011*)

In three dimensions the Calderón problem was addressed and solved in theory in the 1980s. The main ingredients in the solution of the problem are complex geometrical optics solutions to the conductivity equation and a (non-physical) scattering transform. The resulting reconstruction algorithm is in principle direct and addresses the full non-linear problem immediately. In this paper a new simplification of the algorithm is suggested. The method is based on solving a boundary integral equation for the complex geometrical optics solutions, and the method is implemented numerically using a Nyström method. Convergence estimates are obtained using hyperinterpolation operators. We compare the method numerically to two other approximations by evaluation on two numerical examples. In addition a moment method for the numerical solution of the forward problem is given.

Keywords: Calderón problem, Electrical Impedance Tomography, Reconstruction algorithm, Numerical solution, Moment method, Hyperinterpolation

AMS Subject Classification: 35R30, 65N21, 65R32

1. Introduction

The inverse conductivity problem, or the Calderón problem, concerns the unique determination and reconstruction of an electric conductivity distribution in a bounded domain from knowledge of the Dirichlet-to-Neumann (or Voltage-to-Current) map on the boundary of the domain; the problem was first formulated by Calderón in 1980 [1]. Electrical Impedance Tomography (EIT), one of the numerous applications of this problem, is an emerging technology for imaging with for instance applications in medicine [2].

Consider a bounded Lipschitz domain $\Omega \subset \mathrm{R}^3$ having the conductivity distribution $\sigma \in L^\infty(\Omega)$ with $\sigma \geq c > 0$. A given voltage potential $f \in H^{1/2}(\partial\Omega)$ on the surface $\partial\Omega$ gives rise to the voltage potential $u_f \in H^1(\Omega)$ inside Ω, which is given as the unique solution to

$$\begin{aligned} \nabla \cdot \sigma \nabla u_f &= 0 \text{ in } \Omega, \\ u_f &= f \text{ on } \partial\Omega. \end{aligned} \tag{1}$$

The current flux $g_f \in H^{-1/2}(\partial\Omega)$ through the boundary surface is then given by

*Corresponding author. Email: K.Knudsen@mat.dtu.dk

$g_f = \sigma\partial_\nu u_f$ where ν denotes the outward unit normal to $\partial\Omega$. The Dirichlet-to-Neumann map is now given by

$$\Lambda_\sigma : f \mapsto g_f. \tag{2}$$

The Calderón problem asks now: does Λ_σ determine σ uniquely, and in case so, is there a stable reconstruction algorithm for the computation of σ?

In the late 1980s the theory of complex geometrical optics (CGO) solutions to the governing equation was developed and uniqueness for the inverse problem was proved in the smooth case [3]. Later the assumption has been relaxed [4, 5]. Also in the late 1980s the theoretical foundation of a direct reconstruction method was formulated [6, 7]. The algorithm has essentially three steps: first the boundary values of CGO solutions are computed by solving a boundary integral equation, second a scattering transform is computed and an inverse Fourier transform is taken, and finally a boundary value problem is solved for the conductivity distribution.

The 2D Calderón problem was solved for smooth conductivities in [8], and the algorithm was successfully implemented [9–14]. Several ideas from these implementations were used recently in a crude simplification of the reconstruction method for 3D [15, 16]. More recently the Calderón problem in 2D was solved in full generality [17] and implemeted numerically in [18].

Simplifications of the Calderón problem have led to the development of different kinds of imaging algorithms in the framework of EIT. For example, limiting the imaging problem to finding the shape of an inclusion, without trying to get any information on the conductivity, gives rise to qualitative methods like the factorization method [19–21]. Focusing on the reconstruction of inclusions with piecewise constant conductivities can be solved quantitatively by iterative methods [22, 23]. We refer to [24] for the description of other linearization or iteration based reconstruction algorithms.

In this manuscript we develop and investigate several numerical algorithms that can be understood as simplified implementations of the above-mentioned CGO reconstruction method in 3D. In previous implementations, the first step of the reconstruction method was linearized resulting in a Born type reconstruction algorithm. The main novelty of this paper is that we actually implement and solve to first order the boundary integral equation. In addition we develop an accurate numerical algorithm for the solution of the forward problem.

The outline of the paper is as follows. In section 2 we explain the theory behind the reconstruction algorithm and the three simplifications considered here. Next we develop in section 3 an accurate numerical algorithm for the solution of the forward problem based on the moment method. Then in section 4 we give the numerical implementation for the algorithms focusing on the solution of the boundary integral equation. Finally section 5 is devoted to numerical experiments.

Notation: We consider the particular domain $\Omega = B(0,1) \subset \mathrm{R}^3$, the unit ball in R^3. In addition, we suppose that $\sigma \in C^\infty(\overline{\Omega})$ and that $\sigma = 1$ in the neighborhood of $\partial\Omega$. For $\xi \in \mathrm{R}^3$ we define the set

$$\mathcal{V}_\xi = \{\zeta \in \mathrm{C}^3 \mid \zeta^2 = (\xi + \zeta)^2 = 0\}.$$

2. The reconstruction algorithms

In this section we present the theoretical background for the reconstruction algorithm [6, 7] and give three different simplifications of this algorithm.

Let u be a solution to (1) and define $v = \sigma^{1/2}u$. Then v satisfies

$$\begin{aligned} (-\Delta + q)v &= 0 \text{ in } \Omega, \\ v &= f \text{ on } \partial\Omega, \end{aligned} \tag{3}$$

with $q = \Delta\sigma^{1/2}/\sigma^{1/2}$. Since (1) is uniquely solvable, so is (3). Extending q by 0 outside Ω, the reconstruction algorithm is based on the scattering transform of q defined by

$$\mathbf{t}(\xi,\zeta) = \int_\Omega e^{-ix\cdot(\xi+\zeta)}\psi_\zeta(x)q(x)dx, \qquad \xi \in \mathrm{R}^3, \quad \zeta \in \mathcal{V}_\xi, \tag{4}$$

where ψ_ζ denotes the complex geometrical optics solution to

$$(-\Delta + q)v = 0 \text{ in } \mathrm{R}^3, \tag{5}$$

satisfying the asymptotic condition $e^{-ix\cdot\zeta}\psi_\zeta(x) \approx 1$ for large $|x|$. The existence and uniqueness of these solutions are known for large $|\zeta|$ [3] and small $|\zeta|$ [25]. In a sense, $\mathbf{t}$ can be understood as a non-linear Fourier transform of q. In fact

$$|\mathbf{t}(\xi,\zeta) - \hat{q}(\xi)| \leq \frac{C}{|\zeta|},$$

where $\hat{q}$ denotes the Fourier transform of q. Integration by parts in (4) yields

$$\mathbf{t}(\xi,\zeta) = \int_{\partial\Omega} e^{-ix\cdot(\xi+\zeta)}[(\Lambda_\sigma - \Lambda_1)\psi_\zeta](x)\, dS(x). \tag{6}$$

For $\zeta \in \mathcal{V}_\xi$ consider the Faddeev Green's function [26]

$$G_\zeta(x) = \frac{e^{ix\cdot\zeta}}{(2\pi)^3}\int_{\mathrm{R}^3} \frac{e^{ix\cdot\xi}}{|\xi|^2 + 2\xi\cdot\zeta}\, d\xi \ , \ x \in \mathrm{R}^3 \setminus \{0\}, \tag{7}$$

which is a fundamental solution of the Laplace equation, and for $\phi \in H^{-1/2}(\partial\Omega)$ define the single-layer operator $S_\zeta\phi$ by

$$(S_\zeta\phi)(x) = \int_{\partial\Omega} G_\zeta(x-y)\phi(y)\, dS(y) \ , \ x \in \partial\Omega. \tag{8}$$

This operator is bounded from $H^{-1/2}(\partial\Omega)$ to $H^{1/2}(\partial\Omega)$. For $\zeta = 0$ we get the usual fundamental solution of Laplace's equation $G_0(x) = 1/(4\pi|x|)$, and we note that S_0 is the usual single-layer operator.

The reconstruction algorithm consists of three steps:

$$\Lambda_\sigma \ \xrightarrow{\text{(i)}} \ \mathbf{t}(\xi,\zeta) \ \xrightarrow{\text{(ii)}} \ q(x) \ \xrightarrow{\text{(iii)}} \ \sigma(x).$$

(i) $\psi_\zeta|_{\partial\Omega}$ can be computed from Λ_σ from the uniquely solvable boundary integral equation

$$\psi_\zeta + [S_\zeta(\Lambda_\sigma - \Lambda_1)\psi_\zeta] = e_\zeta \ , \ x \in \partial\Omega, \tag{9}$$

where $e_\zeta(x) = e^{ix\cdot\zeta}$. Then $\mathbf{t}$ can be computed by (6).

(ii) q can be computed from $\mathbf{t}$ using

$$\lim_{\zeta\to\infty} \mathbf{t}(\xi,\zeta) = \hat{q}(\xi)\ ,\ \xi\in \mathrm{R}^3,$$

and the inverse Fourier transform.

(iii) σ can be computed from q by solving

$$\begin{aligned}(\Delta+q)\sigma^{1/2} &= 0 \text{ in } \Omega,\\ \sigma^{1/2} &= 1 \text{ on } \partial\Omega.\end{aligned} \tag{10}$$

The $\mathbf{t}^0$ approximation. An approximation $\mathbf{t}^0$ to the function $\mathbf{t}$ can be computed as follows. To avoid working with the exponentially growing Faddeev Green's function in the boundary integral equation (9) we suggest to consider

$$\psi^0_\zeta + S_0(\Lambda_\sigma - \Lambda_1)\psi^0_\zeta = e_\zeta\ ,\ x\in\partial\Omega. \tag{11}$$

It can be shown [25] that (11) is uniquely solvable for any ζ. We then compute $\mathbf{t}^0$ by inserting ψ^0_ζ for ψ in (6), that is

$$\mathbf{t}^0(\xi,\zeta) = \int_{\partial\Omega} e^{-ix\cdot(\xi+\zeta)}[(\Lambda_\sigma-\Lambda_1)\psi^0_\zeta](x)\,dS(x)\ ,\ \xi\in\mathrm{R}^3, \zeta\in\mathcal{V}_\xi. \tag{12}$$

Since $\mathbf{t}^0(\xi,\zeta)$ grows exponentially fast as $|\zeta|\to\infty$ it makes no sense to consider the limit in step (ii) of the algorithm. Instead we propose to fix some vector $\zeta=\zeta_{\mathrm{F}}\in\mathcal{V}_\xi$, consider $\mathbf{t}^0(\xi,\zeta_{\mathrm{F}})$ as the Fourier transform of a potential q^0, and carry out step (iii) of the algorithm as before with q replaced by q^0. We will call the obtained reconstruction σ^0. The specific choice of ζ_{F} will certainly affect the solution. For the 2D problem a similar approximation was used in [27, 28].

The $\mathbf{t}^{\exp}$ approximation. A crude approximation of $\mathbf{t}$ is obtained by substituting the asymptotic value of $\psi_\zeta(x)\approx e^{ix\cdot\zeta}$ for ψ_ζ in (6). This was suggested for the 2D problem in [9, 10] and also used in previous numerical implementations for the 3D problem [15, 16]. The resulting approximation of $\mathbf{t}$ is denoted by $\mathbf{t}^{\exp}$, i.e.

$$\mathbf{t}^{\exp}(\xi,\zeta) = \int_{\partial\Omega} e^{-ix\cdot(\xi+\zeta)}[(\Lambda_\sigma-\Lambda_1)e_\zeta](x)\,dS(x)\ ,\ \xi\in\mathrm{R}^3, \zeta\in\mathcal{V}_\xi. \tag{13}$$

Similar to above, also $\mathbf{t}^{\exp}(\xi,\zeta)$ diverges as $|\zeta|\to\infty$, and hence we propose to fix a vector $\zeta=\zeta_{\mathrm{F}}\in\mathcal{V}_\xi$ and then consider $\mathbf{t}^{\exp}(\xi,\zeta_{\mathrm{F}})$ as the Fourier transform of a potential $q^{\exp}$, and carry out step (ii) of the algorithm as before with q replaced by $q^{\exp}$. This way we obtain an approximation of σ denoted by $\sigma^{\exp}$. Effectively this approach gives a linearization of step (i) in the algorithm.

Remark: When q is replaced by q^0 or $q^{\exp}$, the problem (10) may not be uniquely solvable anymore. In the numerical computations we will assume that uniqueness holds.

The Calderón inversion. Step (ii) in the algorithm above the algorithm is already linear, and step (iii) can be linearized similar to step (i).

For the choice $\zeta = \zeta_{\mathrm{F}} \in \mathcal{V}_\xi$, this gives the reconstruction formula

$$\sigma^{\mathrm{app}}(x) = 1 - \frac{1}{2(2\pi)^n} \int_{\mathrm{R}^3} \frac{\mathbf{t}^{\exp}(\xi, \zeta_{\mathrm{F}})}{|\xi|^2} e^{ix\cdot\xi}\, d\xi \ , \ x \in \Omega, \tag{14}$$

where the integral should be understood as the inverse Fourier transform in the sense of distributions. Calderón's reconstruction method was also implemented for the 3D problem in [15, 16] and in [29], where the method was considered in a 3D mammography geometry, adapted to a setting of electrode measurements taken on part of the boundary, and tested on tank data.

3. Numerical computation of the Dirichlet-to-Neumann map

This section describes the numerical solution of the forward problem. The numerical implementation proposed in section 4 of the reconstruction algorithms presented in section 2 makes use of values of $\Lambda_\sigma Y_d^k$ at well-chosen points on the unit sphere for spherical harmonics Y_d^k up to a certain degree $d = N$. We propose to solve the forward problem taking advantage of the geometry and the special form of Dirichlet data to build the discretized Dirichlet-to-Neumann map with a good accuracy. Thus, the numerical scheme for solving the PDE is based on the equivalent reformulation of the problem as an integral equation that takes into account the particular geometry and the special Dirichlet data. This integral equation is then solved accurately using the well-known moment method [30]. Numerically, for fixed d, k, we will represent $\Lambda_\sigma Y_d^k$ as

$$\Lambda_\sigma Y_d^k \simeq \sum_{n=0}^{N'} \sum_{m=-n}^{n} \lambda_n^m Y_n^m, \tag{15}$$

with coefficients $\lambda_n^m \in \mathrm{C}$. The integer N' is fixed in the choice of the approximation space in the moment method. Note that λ_n^m depends implicitly on d, k. Instead of solving (1) with Dirichlet data $f = Y_d^k$ directly, we solve the Schrödinger equation

$$\begin{aligned} -\Delta v + qv &= 0 \quad \text{in } \Omega, \\ v &= Y_d^k \quad \text{on } \partial\Omega. \end{aligned} \tag{16}$$

3.1. *Integral equation arising from the generalized Laplace equation*

Consider the solution $\tilde{v}$ to the Laplace equation

$$\begin{aligned} -\Delta \tilde{v} &= 0 \quad \text{in } \Omega, \\ \tilde{v} &= Y_k^d \quad \text{on } \partial\Omega. \end{aligned} \tag{17}$$

In spherical coordinates (r, θ, φ) the solution is simply given by

$$\tilde{v}(r, \theta, \varphi) = r^d Y_d^k(\theta, \varphi). \tag{18}$$

If $v, \tilde{v}$ denote the solutions to (16) and (17) respectively, $w = v - \tilde{v} \in H^1(\Omega)$ solves

$$\begin{aligned} -\Delta w + qw &= -q\tilde{v} \quad \text{in } \Omega, \\ w &= 0 \quad \text{on } \partial\Omega. \end{aligned} \tag{19}$$

Introduce the Dirichlet Green's function for the Laplacian in the unit ball given by

$$G_0^{\mathrm{D}}(x,y) = G_0(x-y) - G_0(|y|(x-y/|y|^2)) \ , \ x,y \in \Omega, x \neq y. \tag{20}$$

Then (19) is equivalent to

$$(I+V)w = -V\tilde{v}, \tag{21}$$

where

$$V\colon w \mapsto \int_\Omega G_0^{\mathrm{D}}(x,y)q(y)w(y)\,dy \ , \ x \in \Omega.$$

Since (16) is uniquely solvable, so is the integral equation (21).

3.2. *Numerical solution of the integral equation* (21)

Consider in $L^2(\Omega)$ the orthonormal basis

$$\Upsilon_{n,m,\ell}(r,\theta,\varphi) = \frac{\sqrt{2}}{j_{n+1}(\mu_{n,\ell})} j_n(\mu_{n,\ell}r)Y_n^m(\theta,\varphi), n \in \mathrm{N}, |m| \leq n, \ell \in \mathrm{N} \tag{22}$$

consisting of eigenfunctions for the Dirichlet Laplacian in Ω. Here $j_n, n \in \mathrm{N}$, denotes the n'th spherical Bessel functions, and $\mu_{n,\ell} > 0$ are the positive zeros of j_n arranged in increasing order. Since the eigenvalue corresponding to $\Upsilon_{n,m,\ell}$ is $\mu_{n,\ell}^2$, it follows that

$$\int_\Omega G_0^{\mathrm{D}}(x,y)\Upsilon_{n,m,\ell}(y)\,dy = \frac{\Upsilon_{n,m,\ell}(x)}{\mu_{n,\ell}^2} \ , \ x \in \Omega,$$

and hence

$$V^*\Upsilon_{n,m,\ell} = q\frac{\Upsilon_{n,m,\ell}}{\mu_{n,\ell}^2}. \tag{23}$$

Consider positive integers N' and L' and define the space of test functions

$$\mathrm{P}_{N',L'} = \mathrm{span}\{\Upsilon_{n,m,\ell} : n \leq N', |m| \leq n, \ell \leq L'\},$$

and define in addition the approximation space

$$\mathrm{P}_{N',L'}^V = (I+V^*)\mathrm{P}_{N',L'}.$$

We will approximate the solution w to (21) by

$$w_{N',L'} = \sum_{n'=0}^{N'} \sum_{m'=-n'}^{n'} \sum_{\ell'=0}^{L'} W_{n',m',\ell'}(I+V^*)\Upsilon_{n',m',\ell'}, \tag{24}$$

and we require that $w_{N',L'}$ satisfies (21) in the sense that

$$\langle (I+V)w_{N',L'}, \Upsilon\rangle = \langle -V\tilde{v}, \Upsilon\rangle \quad \text{for all} \quad \Upsilon \in \mathrm{P}_{N',L'}, \tag{25}$$

where $\langle \cdot, \cdot \rangle$ denotes the usual inner product in $L^2(\Omega)$. Inserting $\Upsilon = \Upsilon_{n,m,\ell}$ as test functions in (25) and using (23) the left hand side equals

$$\begin{aligned}\langle (I+V)w_{N',L'}, \Upsilon_{n,m,\ell}\rangle &= \sum_{n'=0}^{N'} \sum_{m'=-n'}^{n'} \sum_{\ell'=0}^{L'} W_{n',m',\ell'} \langle (I+V^*)\Upsilon_{n',m',\ell'}, (I+V^*)\Upsilon_{n,m,\ell}\rangle \\ &= \sum_{n'=0}^{N'} \sum_{m'=-n'}^{n'} \sum_{\ell'=0}^{L'} W_{n',m',\ell'} \left\langle \left(1+\frac{q}{\mu_{n',\ell'}^2}\right)\Upsilon_{n',m',\ell'}, \left(1+\frac{q}{\mu_{n,\ell}^2}\right)\Upsilon_{n,m,\ell}\right\rangle. \end{aligned} \tag{26}$$

To evaluate the right hand side we expand $\tilde{v}$ in the basis $\Upsilon_{n',m',\ell'}$. Since

$$\frac{\sqrt{2}}{j_{d+1}(\mu_{d,\ell'})}\int_0^1 r^{d+2} j_d(\mu_{d,\ell'} r)\, dr = \frac{\sqrt{2}}{\mu_{d,\ell'}}\ ,\ \ell' \in \mathrm{N},$$

we obtain

$$\tilde{v} = \sum_{\ell'=0}^{\infty} \frac{\sqrt{2}}{\mu_{d,\ell'}} \Upsilon_{d,k,\ell'}.$$

Hence,

$$\begin{aligned}\langle -V\tilde{v}, \Upsilon_{n,m,\ell}\rangle &= -\langle \tilde{v}, V^*\Upsilon_{n,m,\ell}\rangle \\ &= -\left\langle \tilde{v}, \frac{q}{\mu_{n,\ell}^2}\Upsilon_{n,m,\ell}\right\rangle \\ &= -\sum_{\ell'=0}^{\infty} \frac{\sqrt{2}}{\mu_{d,\ell'}} \left\langle \Upsilon_{d,k,\ell'}, \frac{q}{\mu_{n,\ell}^2}\Upsilon_{n,m,\ell}\right\rangle, \end{aligned} \tag{27}$$

which we truncate at $\ell' = L'$. Inserting (26) and (27) in (25) yields a matrix equation for the coefficients $W_{n',m',\ell'}$. To be explicit, we replace the indices (n, m, ℓ) and (n', m', ℓ') by the single indices i and i' given by

$$\begin{aligned} i &= (L'+1)n^2 + (\ell+1)(n+m) + (\ell+1), \\ i' &= (L'+1)n'^2 + (\ell'+1)(n'+m') + (\ell'+1), \end{aligned}$$

and let $\underline{W}$ denote the vector with elements

$$\underline{W}_{i'} = W_{n',m',\ell'}.$$

Then $\underline{W}$ satisfies the matrix equation

$$\underline{W} + R\underline{W} + R^*\underline{W} + S\underline{W} = -R\underline{h}, \tag{28}$$

where the matrices R, S have elements

$$R_{i,i'} = \frac{1}{\mu_{n,\ell}^2} \int_\Omega q(x) \Upsilon_{n',m',\ell'}(x) \overline{\Upsilon}_{n,m,\ell}(x)\, dx, \tag{29}$$

$$S_{i,i'} = \frac{1}{\mu_{n,\ell}^2 \mu_{n',\ell'}^2} \int_\Omega q^2(x) \Upsilon_{n',m',\ell'}(x) \overline{\Upsilon}_{n,m,\ell}(x)\, dx, \tag{30}$$

and $\underline{h}$ has elements

$$h_{i'} = \begin{cases} \dfrac{\sqrt{2}}{\mu_{n',\ell'}} & \text{if } n' = d \text{ and } m' = k \\ 0 & \text{if } n' \neq d \text{ or } m' \neq k \end{cases}.$$

We emphasize that the matrices S and $I+R+R^*+S$ involved in (28) are Hermitian, and that $\underline{h}$ is a sparse vector. This is utilized in the numerical implementation.

3.3. *Computation of matrix elements*

Computation of the matrix elements in (29) and (30) involves integrals in the unit ball. These integrals are computed (following [31, p. 79]) using a quadrature rule adapted to integration in spherical coordinates. For $n, \ell \in \mathrm{N}$, we will denote by P_n, the Legendre polynomial of degree n and $P_\ell^{(0,2)}$ the Jacobi polynomials of degree ℓ for parameters $(0, 2)$.

Consider a positive integer N'' and the $2(N''+1)^2$ points $x_{m,n}$ on the unit sphere $\partial\Omega$, with $0 \leq m \leq N'', 0 \leq n \leq 2N''+1$, given by the spherical coordinates

$$x_{m,n} = (\sin\theta_m \cos\varphi_n, \sin\theta_m \sin\varphi_n, \cos\theta_m)\,, \tag{31}$$

where $\theta_m = \arccos t_m$ and $\varphi_n = \pi n/(N''+1)$, the real numbers t_m being the increasing $N''+1$ zeros of $P_{N''+1}$.

Then, considering the weights $\alpha_m = \dfrac{2(1-t_m^2)}{(N''+1)^2[P_{N''}(t_m)]^2}$ of the Gauss-Legendre quadrature rule of order $N''+1$ on $[-1,1]$, the following quadrature rule on the sphere integrates exactly spherical harmonics of degree less than or equal to $2N''+1$

$$\int_{\partial\Omega} \phi\, ds \simeq \frac{\pi}{N''+1} \sum_{m=0}^{N''} \sum_{n=0}^{2N''+1} \alpha_m \phi(x_{m,n})\ ,\ \phi \in C^0(\partial\Omega). \tag{32}$$

Consider now a positive integer L'' and the nodes r_ℓ and weights β_ℓ, with $\ell = 0 \ldots L''$, of quadrature rule of order $L''+1$ on $[0,1]$, with weighting function $\omega(r) = r^2$, that is, r_ℓ are the increasing $L''+1$ zeros of $P_{L''+1}^{(0,2)}(2X-1)$ and $\beta_\ell = \dfrac{(L''+2)^2(1-(2r_\ell-1)^2)}{(L''+1)^2(L''+3)^2[P_{L''}^{(0,2)}(2r_\ell-1)]^2}$.

Then, for $\Phi \in C^0(\Omega)$, the integral of Φ is approximated by the following quadrature rule

$$\int_{r=0}^1 \int_{\theta=0}^{\pi} \int_{\varphi=0}^{2\pi} \Phi(r,\theta,\phi) r^2 \sin\theta\, dr d\theta d\varphi \simeq \frac{\pi}{N''+1} \sum_{\ell=0}^{L''} \sum_{m=0}^{N''} \sum_{n=0}^{2N''+1} \alpha_\ell \beta_m \Phi(r_\ell, \theta_m, \varphi_n). \tag{33}$$

In practice, all matrix elements involve q, which is of limited support, so that the number of quadrature points really used is lower than the total number $2(L''+1)(N''+1)^2$ of quadrature points in the unit ball.

3.4. *Back to the Dirichlet-to-Neumann map*

After computing the matrices in (28) using (33), we solve the linear system (28). Hence we get an approximation w of the solution to the integral equation (21) given by (24), and the approximated solution v of (16) is given by

$$v_{N',L'}(r,\theta,\varphi) = \tilde{v}(r,\theta,\varphi) + w_{N',L'}(r,\theta,\varphi).$$

However, we only need to compute the normal trace of u at the quadrature points on the unit sphere, chosen for the inversion algorithm. Since

$$\left(\frac{d}{dr} j_n(\mu_{n,\ell} r)\right)\Big|_{r=1} = -\mu_{n,\ell} j_{n+1}(\mu_{n,\ell})$$

we find on $\partial\Omega$

$$\Lambda_\sigma Y_d^k \simeq dY_d^k - \sqrt{2}\sum_{n=0}^{N'}\sum_{m=-n}^{n}\sum_{\ell=0}^{L'} \mu_{n,\ell} W_{n,m,\ell} Y_n^m, \tag{34}$$

which can also be written as

$$(\Lambda_\sigma - \Lambda_1) Y_d^k \simeq -\sqrt{2}\sum_{n=0}^{N'}\sum_{m=-n}^{n}\sum_{\ell=0}^{L'} \mu_{n,\ell} W_{n,m,\ell} Y_n^m. \tag{35}$$

3.5. *Implementation tools*

Computations for the forward problem are implemented in C++, using the Boost C++ Libraries [32] for matrices and vectors classes and for special functions. System solving is done using the LAPACK library [33]. In order to speed up matrices computations, a hybrid programming using OpenMP® [34] and Open MPI [35] for parallelization, has been implemented.

4. Numerical implementation of the reconstruction algorithms

4.1. *Numerical solution of the boundary integral equation*

In order to solve the boundary integral equations (11), we tailor the Nyström type method [36] (see also [31, section 3.6]) to the particular geometry and operators. The resulting algorithm has super-algebraic convergence with respect to the number of discretization points, that is, the convergence is faster than any power of the inverse of the number of discretization points.

Consider a positive integer N, let H_N denote the linear space spanned by spherical harmonics of degree less than or equal to N, and let T_N denote the $L^2(\partial\Omega)$

orthogonal projector onto H_N. Then, for all $\phi \in L^2(\partial\Omega)$

$$T_N\phi = \sum_{n=0}^{N} \sum_{m=-n}^{n} \langle \phi, Y_n^m \rangle Y_n^m,$$

where $\langle \cdot, \cdot \rangle$ denotes the $L^2(\partial\Omega)$ inner product. For a continuous function ϕ, the inner products can be approximated using the quadrature formula (32). This motivates an approximation of T_N by the operator L_N defined by

$$L_N\phi = \frac{\pi}{N+1} \sum_{n=0}^{N} \sum_{m=-n}^{n} \sum_{k=0}^{N} \sum_{\ell=0}^{2N+1} \alpha_k \phi(x_{k\ell}) Y_n^{-m}(x_{k,\ell}) Y_n^m \ , \ \phi \in C^0(\partial\Omega). \tag{36}$$

The operator L_N is called the hyperinterpolation operator (see [37] where L_N was first introduced), and it is a projection operator from $L^2(\partial\Omega)$ onto H_N. Hyperinterpolation on the sphere, but also on general manifolds and in higher dimensions, has been widely studied and the error $\phi - L_N\phi$ estimated in different norms, in particular, to prove convergence of the numerical solution to the noudary integral equation, we will make use of estimates in Sobolev norms proved in [38]. For all $n \in \mathrm{N}$ and $|m| \leq n$, we have

$$\frac{1}{4\pi} \int_{\partial\Omega} \frac{Y_n^m(y)}{|x-y|} \, dS(y) = \frac{1}{2n+1} Y_n^m(x) \ , \ x \in \partial\Omega.$$

Hence, for $\phi \in C^0(\partial\Omega)$, using the approximation $L_N\phi$ of ϕ and the addition theorem for spherical harmonics [31, (2.29)], we get

$$[S_0\phi](x) \simeq [S_0 L_N \phi](x) = \frac{1}{4(N+1)} \sum_{k=0}^{N} \sum_{\ell=0}^{2N+1} \alpha_k \phi(x_{k,\ell}) \sum_{n=0}^{N} P_n(x_{k,\ell} \cdot x) \ , \ x \in \partial\Omega. \tag{37}$$

Since $H^s(\partial\Omega)$ is continuously embedded in $C^0(\partial\Omega)$ for $s > 1$, $L_N\phi$ is well-defined for $\phi \in H^s(\partial\Omega), s > 1$, and in particular $L_N\phi \in H^s(\partial\Omega)$. Moreover, since $\sigma = 1$ near the unit sphere $\partial\Omega$, the operator $\Lambda_\sigma - \Lambda_1$ is in fact infinitely smoothing, i.e. it maps any Sobolev space $H^s(\partial\Omega)$ to $H^{s+t}(\partial\Omega)$ for any $s \geq 1/2$ and $t \in \mathrm{R}$ (see [25] for a proof). So $L_N(\Lambda_\sigma - \Lambda_1)\phi$ is also well-defined in $H^s(\partial\Omega)$ for $\phi \in H^s(\partial\Omega)$ with $s > 1$. We will approximate the solution ψ_ζ^0 of (11) by the solution ψ^N of

$$[I + S_0 L_N(\Lambda_\sigma - \Lambda_1) L_N]\psi^N = e_\zeta. \tag{38}$$

First we will study the solvability of (38) and show a convergence result for the solution of the discretized problem. Then we will give the numerical implementation.

Lemma 4.1: *Let $s > 5/2$, then there exists a constant C such that*

$$\|S_0(\Lambda_\sigma - \Lambda_1) - S_0 L_N(\Lambda_\sigma - \Lambda_1) L_N\|_{H^s(\partial\Omega) \to H^s(\partial\Omega)} \leq \frac{C}{N^{s-5/2}} \tag{39}$$

for all $N \in \mathrm{N}$.

Proof: Let $s > 5/2$ and $N \in \mathrm{N}$. Denote $\tilde{\Lambda} = \Lambda_\sigma - \Lambda_1$ and consider $\phi \in H^s(\partial\Omega)$.

$$\begin{aligned}&\|(S_0\tilde{\Lambda} - S_0 L_N \tilde{\Lambda} L_N)\phi\|_{H^s(\partial\Omega)} \leq \\ &\|S_0(I - L_N)\tilde{\Lambda}\phi\|_{H^s(\partial\Omega)} + \|S_0 L_N \tilde{\Lambda}(I - L_N)\phi\|_{H^s(\partial\Omega)}\end{aligned} \tag{40}$$

Considering the first part of the right hand side in (40), we have

$$\|S_0(I - L_N)\tilde{\Lambda}\phi\|_{H^s(\partial\Omega)} \leq \|S_0\|_{H^{s-1}(\partial\Omega)\to H^s(\partial\Omega)}\|(I - L_N)\tilde{\Lambda}\phi\|_{H^{s-1}(\partial\Omega)}.$$

And using estimates in Theorem 3.4 of [38], we get

$$\|S_0(I - L_N)\tilde{\Lambda}\phi\|_{H^s(\partial\Omega)} \leq \frac{C}{N^{t-s}}\|S_0\|_{H^{s-1}(\partial\Omega)\to H^s(\partial\Omega)}\|\tilde{\Lambda}\phi\|_{H^t(\partial\Omega)}$$

for all $t \geq s-1$, C being independent of N. Hence, using the smoothing properties of $\tilde{\Lambda}$ and choosing $t = 2s - 5/2$, we have

$$\|S_0(I - L_N)\tilde{\Lambda}\phi\|_{H^s(\partial\Omega)} \leq \frac{C'}{N^{s-5/2}}\|\phi\|_{H^s(\partial\Omega)} \tag{41}$$

where C' is a constant independent of N.

Consider now the second part of the right hand side in (40). We have

$$\begin{aligned}&\|S_0 L_N \tilde{\Lambda}(I - L_N)\phi\|_{H^s(\partial\Omega)} \\ &\quad\leq \|S_0\|_{H^{s-1}(\partial\Omega)\to H^s(\partial\Omega)}\|L_N\|_{H^t(\partial\Omega)\to H^{s-1}(\partial\Omega)}\|\tilde{\Lambda}\|_{H^{3/2}(\partial\Omega)\to H^t(\partial\Omega)}\|(I - L_N)\phi\|_{H^{3/2}(\partial\Omega)}\end{aligned}$$

for all $t \geq s-1$. Thus, choosing $t = s$ and using estimates of Theorem 3.4 of [38], we have

$$\|S_0 L_N \tilde{\Lambda}(I - L_N)\phi\|_{H^s(\partial\Omega)} \leq \frac{C''}{N^{s-5/2}}\|\phi\|_{H^s(\partial\Omega)} \tag{42}$$

where C'' is a constant independent of N. Combining (40), (41), (42) ends the proof. □

We now give the convergence results on solutions of the discretized problem (38).

Theorem 4.2: *For all $s > 5/2$, there exists $N_0 \in \mathrm{N}$ (depending on s), such that for all $N \geq N_0$, the operator $I + S_0 L_N(\Lambda_\sigma - \Lambda_1)L_N$ is invertible in $H^s(\partial\Omega)$. Moreover, for the solution $\psi^0_\zeta \in H^s(\partial\Omega)$ to (11) and the solution $\psi^N \in H^s(\partial\Omega)$ to the discretized problem (38) for $N \geq N_0$, we have*

$$\|\psi^N - \psi^0_\zeta\|_{H^s(\partial\Omega)} \leq \frac{C}{N^{s-5/2}}\|e_\zeta\|_{H^s(\partial\Omega)}$$

where C depends only on s.

Proof: The discretized operator $I + S_0 L_N(\Lambda_\sigma - \Lambda_1)L_N$ is for large N due to (39) a small perturbation of the invertible operator $I + S_0(\Lambda_\sigma - \Lambda_1)$. Hence it is invertible by a Neumann series, from which also the norm estimate follows. □

Next, we will see that problem (38) sums up to solving a finite-dimensional linear

system. Let N be a positive integer and denote by B the matrix of the operator

$$\begin{aligned}\mathrm{C}^{2(N+1)^2} &\to \mathrm{C}^{2(N+1)^2}\\ \underline{\phi} &\mapsto \frac{\pi}{N+1}\sum_{n=0}^{N}\sum_{m=-n}^{n}\sum_{k'=0}^{N}\sum_{\ell'=0}^{2N+1}\alpha_{k'}\underline{\phi}_{k',\ell'}Y_n^{-m}(x_{k',\ell'})[(\Lambda_\sigma-\Lambda_1)Y_n^m](x_{k,\ell})\\ &\quad k=0\dots N, \ell=0\dots 2N+1.\end{aligned} \tag{43}$$

So that, for all $\phi \in H^s(\partial\Omega)$ with $s>1$, we have $[(\Lambda_\sigma-\Lambda_1)L_N\phi](x_{k,\ell}) = [B\underline{\phi}]_{k,\ell}$ where $\underline{\phi}$ is the vector of elements $\underline{\phi}_{k,\ell} = \phi(x_{k,\ell})$.

Consider the functions $\omega_{k,\ell}^N$ defined on $\partial\Omega$ by

$$\omega_{k,\ell}^N(x) = \frac{\alpha_k}{4(N+1)}\sum_{n=0}^{N} P_n(x_{k,\ell}\cdot x)\ ,\ x\in\partial\Omega. \tag{44}$$

Let $\chi \in H^s(\partial\Omega)$ with $s>1$, then, if $\phi\in H^s(\partial\Omega)$ is a solution of $[I+S_0L_N(\Lambda_\sigma-\Lambda_1)L_N]\phi=\chi$, the vector $\underline{\phi}_{k,\ell}=\phi(x_{k,\ell})$ satisfies the linear system

$$\underline{\phi}_{k,\ell}+\sum_{k'=0}^{N}\sum_{\ell'=0}^{2N+1}\omega_{k',\ell'}^N(x_{k,\ell})[B\underline{\phi}]_{k',\ell'} = \chi(x_{k,\ell})\ ,\ k=0\dots N,\ell=0\dots 2N+1. \tag{45}$$

Conversely, if $\underline{\phi}\in\mathrm{C}^{2(N+1)^2}$ is a solution of (45), then the function $\phi\in H^s(\partial\Omega)$ defined by

$$\phi(x) = \chi(x) - \sum_{k=0}^{N}\sum_{\ell=0}^{2N+1}\omega_{k,\ell}^N(x)[B\underline{\phi}]_{k,\ell}\ ,\ x\in\partial\Omega$$

is a solution of $[I+S_0L_N(\Lambda_\sigma-\Lambda_1)L_N]\phi=\chi$.

Remark: As we can see in equations (43) and (45), the chosen discretization of the problem implies that the forward data used in the inverse scheme are $[\Lambda_\sigma Y_n^m](x_{k,\ell})$ for $n=0\dots N, |m|\le N, k=0\dots N, \ell=0\dots 2N+1$.

4.2. *The inverse Fourier transform and resolution*

In all three simplifications we need to evaluate the inverse Fourier transform to compute the potentials q^0, $q^{\exp}$, and conductivity σ^{app} from the scattering transforms. We will evaluate the scattering transform on an equidistant mesh in a box $[-\xi_{\mathrm{M}},\xi_{\mathrm{M}}]^3$ for some chosen maximal frequency ξ_{M}, and approximate the inverse Fourier transform using the inverse discrete Fourier transform (implemented by FFT). Since we know that q^0, $q^{\exp}$, and $\sigma^{\mathrm{app}}-1$ are supported in $\Omega=B(0,1)$, we compute these functions on an equidistant grid in $[-1,1]^3$. By comparing the Fourier transform and discrete Fourier series (implemented by FFT) we achieve an upper bound on the number K^3 of points in the reconstructions. Indeed,

$$\xi_{\mathrm{M}} = K\frac{\pi}{2}. \tag{46}$$

Effectively the number of points gives an upper limit for the resolution by this implementation in terms of the mesh-size $2/K=\pi/\xi_{\mathrm{M}}$ in the x-mesh.

4.3. *The Computational Algorithms*

Here we briefly summarize the numerical algorithms developed above. The three algorithms have been implemented using MATLAB®.

The $\mathbf{t}^0$ approximation.

- Build the matrix implementation (45) of the operator $I + S_0(\Lambda_\sigma - \Lambda_1)$.
- Decide upon the upper limit ξ_{M} on $|\xi|$ and compute the number of evaluation points K^3 to be used in FFT given by (46). Create a computational mesh inside $[-\xi_{\text{M}}, \xi_{\text{M}}]^3$ with mesh-size $2\xi_{\text{M}}/K$. This is the mesh for the evaluation of $\mathbf{t}^0$.
- For fixed grid point ξ, compute $\zeta = \zeta_{\min} \in \mathcal{V}_\xi$ with minimal norm. Then solve (45) for the grid approximation of ψ^0_ζ and evaluate $\mathbf{t}^0$ using the integral (12) using the quadrature rule (32).
- Use FFT to compute the inverse Fourier transform of $\mathbf{t}^0(\xi, \zeta_{\min})$ to get a grid approximation of q^0 on a mesh in $[-1, 1]^3$.
- Use a finite element method to solve the Schrödinger equation (10) to get σ^0.

Note that the choice of $\zeta = \zeta_{\min}$ of minimal norm is taken to limit the effect of numerical truncation and rounding errors. Note also that we instead of solving (10) using the numerical scheme given in section 3, we use a different finite element method to avoid the danger of committing inverse crimes.

The $\mathbf{t}^{\exp}$ approximation. The reconstruction scheme for the $\mathbf{t}^{\exp}$ method does not require to solve the first boundary integral equation, hence the steps are:

- Compute (13) using (32) for $|\xi| < \xi_{\text{M}}$, where $\xi_{\text{M}} > 0$ is as before and $\zeta = \zeta_{\min}$ is chosen of minimal norm to avoid numerical instabilities.
- Use FFT to compute the inverse Fourier transform of $\mathbf{t}^{\exp}(\xi, \zeta_{\min})$ to get an approximation $q^{\exp}$ of q.
- Use a finite element method to solve the Schrödinger equation (10) to get $\sigma^{\exp}$.

The Calderón inversion. This scheme does not require the solution of the Schrödinger equation, since the approximation of the conductivity is directly computed from $\mathbf{t}^{\exp}$. Hence the steps are limited to:

- Compute (13) using (32) for $|\xi| < \xi_{\text{M}}$, where $\xi_{\text{M}} > 0$ and $\zeta = \zeta_{\min}$ is chosen of minimal norm to avoid numerical instabilities.
- Use the FFT to compute the inverse Fourier transform of $\mathbf{t}^{\exp}(\xi, \zeta_{\min})/|\xi|^2$ to get $1 - \sigma^{\text{app}}$.

5. Numerical results

5.1. *Radial profile*

As a first test we consider a smooth radial symmetric conductivity with support in the sphere of radius 1/2. The profile of the conductivity is seen in the left panel of figure 1 as (the solid black curve). We take $N = 15$, that is, 512 points on the unit sphere and compare the three reconstruction methods. To compute a matrix approximation of the Dirichlet-to-Neumann map we use the fact that the spherical harmonics are eigenfunctions of the map. The eigenvalues can then be computing as explained in [15]. The approximations of the Fourier transform $\hat{q}$ are plotted in the left panel of figure 1 and compared to the exact Fourier transform and the exact $\mathbf{t}$ for minimal $\zeta_{\min}$. The corresponding reconstructions of the conductivity σ with two different truncation parameters for the scattering and Fourier transforms are shown in the middle and right panel of figure 1.

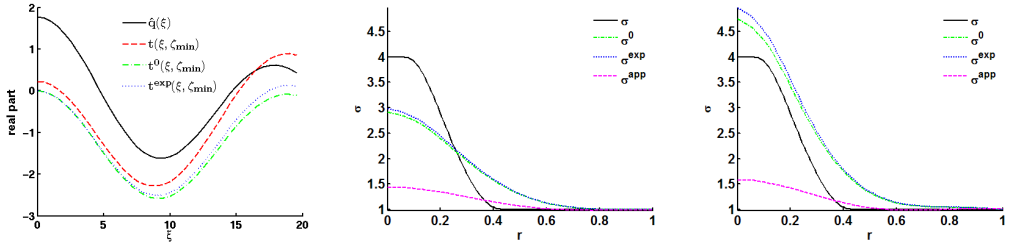

Figure 1. Left: approximations of $\hat{q}$. Middle and right: reconstructions of σ with truncation $\xi_{\mathrm{M}} = 8$ (middle) and $\xi_{\mathrm{M}} = 9$ (right).

In order to study the stability of the methods with respect to noise in the data, we propose to simulate errors on measurements by adding Gaussian noise to the forward data. Considering the discretized Dirichlet-to-Neumann map, represented by the matrix B^σ as in formula (43), where $\Lambda_\sigma - \Lambda_1$ is replaced by Λ_σ, and roughly considering the entries of the matrix as measurements taken at point electrodes located at the quadrature points on the sphere, it appears quite appropriate to add Gaussian noise independently on each elements $B^\sigma_{p,p'}, p, p' = 1 \dots 2(N+1)^2$ of the matrix B^σ, with amplitude depending on matrix elements. Hence, we will represent the noisy discretized Dirichlet-to-Neumann map by a matrix $\tilde{B}^\sigma$ with elements $\tilde{B}^\sigma_{p,p'}, p, p' = 1 \dots 2(N+1)^2$ given by

$$\tilde{B}^\sigma_{p,p'} = B^\sigma_{p,p'} + \delta \epsilon_{p,p'} B^\sigma_{p,p'} \ , \ p, p' = 1 \dots 2(N+1)^2, \tag{47}$$

where δ is the level of noise and $\epsilon_{p,p'}, p, p' = 1 \dots 2(N+1)^2$ are the realizations of $4(N+1)^4$ independent standard normal random variables.

The Fourier transform $\hat{q}$ and the exact $\mathbf{t}$ for minimal $\zeta_{\min}$ are again compared to $\mathbf{t}^0$ and $\mathbf{t}^{\exp}$ approximations reconstructed with different levels of noise (figure 2). As expected, due to the exponentially growing term, the noise in the data implies a blow up of the approximations of the Fourier transform, which happens sooner as the level of noise increases. In figure 3, corresponding reconstructions of the conductivity σ with adapted truncation are shown.

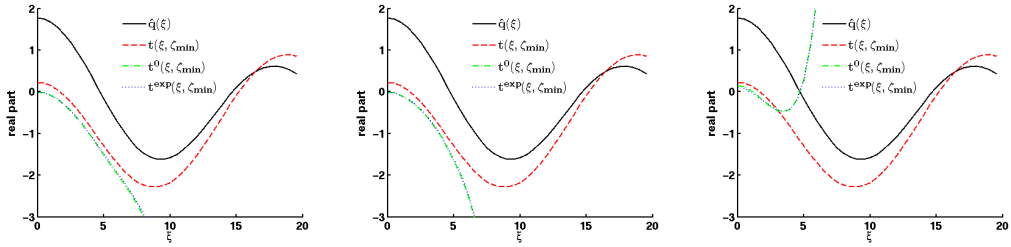

Figure 2. Approximations of $\hat{q}$ in case of noise in the data: left 0.1% noise, middle 1% noise, and right 5% noise.

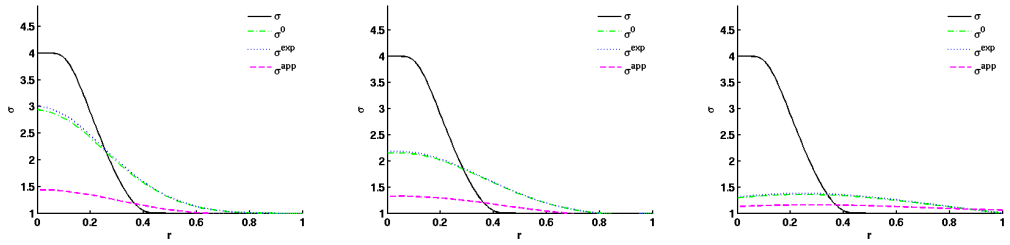

Figure 3. Reconstructions of σ with truncation: left 0.1% noise and $\xi_{\mathrm{M}} = 8$, middle 1% noise and $\xi_{\mathrm{M}} = 7$, and right 5% noise and $\xi_{\mathrm{M}} = 6$.

5.2. *Non-radial profile*

To test the different reconstruction schemes we chose a numerical phantom composed of three objects with constant conductivity different from the unit conductivity of the background medium, see figure 4.

- A ball with center in the (Oxy) plane and with a conductivity larger than 1.
- Two prolate ellipsoids with axis in the (Oxy) plane, with slightly different sizes and with a same conductivity smaller than 1.

In order to be in the framework of the theory, the conductivity distribution must be smooth. Hence we have smoothed out the discontinuities in the phantom. A cross sectional plot of the resulting conductivity distribution and its support can be seen in figure 4.

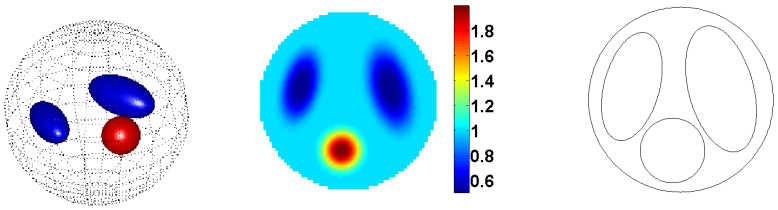

Figure 4. Left: 3D plot of phantom. Middle: profile of the conductivity σ in the (Oxy) plane. Right: support of σ.

We take $N = 15$, that is, 512 points on the unit sphere for reconstructions. The forward data $[\Lambda_\sigma Y_n^m](x_{k,\ell})$, for $n = 0 \dots N, |m| \leq n, k = 0 \dots N, \ell = 0 \dots 2N + 1$, are computed using the method described in section 3 with $N' = 15$ and $L' = 15$ (subsection 3.2) for all $n = 0 \dots N$ and $|m| \leq n$. The matrices (29) and (30) (subsection 3.2) are computed using $N'' = 63$ and $L'' = 63$ for the number of quadrature points in (33) (subsection 3.3).

We consider reconstructions with $\mathbf{t}^0$ and $\mathbf{t}^{\exp}$ approximations and with the Calderón inversion, first with $|\xi| \leq 6$ and then with $|\xi| \leq 8$. The cross sectional profile of the reconstructions for the cases $|\xi| \leq 6$ and $|\xi| \leq 8$ can be seen in figure 5 and 6 respectively.

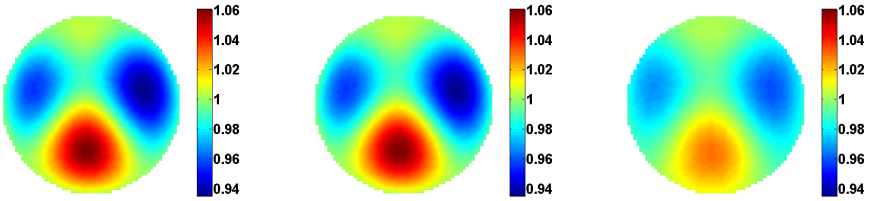

Figure 5. Reconstructions with truncation $\xi_{\mathrm{M}} = 6$: left σ^0, middle σ^{exp}, and right σ^{app}.

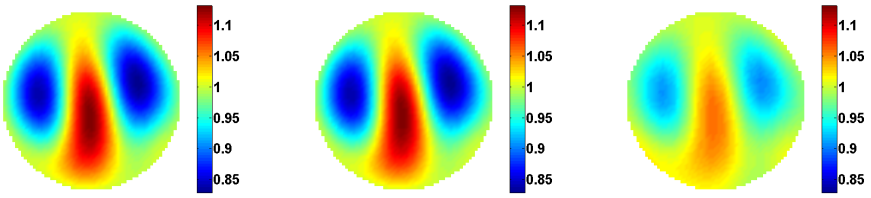

Figure 6. Reconstructions with truncation $\xi_{\mathrm{M}} = 8$: left σ^0, middle σ^{exp}, and right σ^{app}.

We see that the shape of the inclusions is determined better with the lower value of ξ_{M}, whereas the contrast is better achieved with the larger value of ξ_{M}. This is perhaps due to the exponential growth of the involved functions with respect to ξ. Also, we see that even though the reconstructions are quite similar, the reconstructions σ^0 and σ^{exp} seem to be slightly better than σ^{app}. This holds true with both truncations.

In a last numerical experiments, see figure 7, we compute reconstructions with truncation $|\xi| \leq 6$ with different level of gaussian noise added to the forward data.

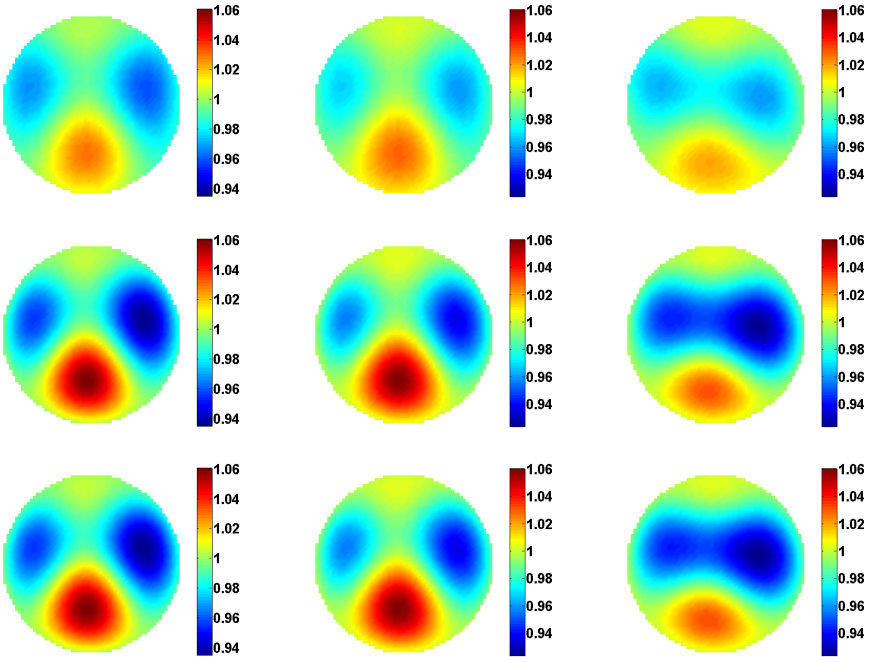

Figure 7. Reconstructions with different noise levels: left column 0%, middle column 0.1% and right column 1%. Upper row σ^{app}, middle row σ^{exp}, and lower row σ^0. Truncation is at $\xi_{\mathrm{M}} = 6$.

6. Conclusions

We have described three different numerical simplifications and implementations of a reconstruction method for the Calderón problem and given their numerical implementations. The performance of the methods was illustrated with a radial conductivity and a phantom consisting of three inclusions. All three methods produce reconstructions that separate and localize the inclusions, however the contrast is not reliable. This fact is due to the spectral truncation at low frequency necessary for producing stable reconstructions. A comparison of the three methods shows that the mere linearization performs the poorest, whereas the most involved method based on solving the perturbed boundary integral equation gives the best reconstructions. However, there is still room for improvement, and this may be achieved by solving the correct boundary integral equation as a first step in the algorithm. The numerical examples show that there is a delicate balance between the noise in the problem, the errors in the computation, and the truncation of the scattering transform, but more analysis must be done to reveal the connections and understand the regularization effect of the truncation.

Acknowledgments

Fabrice Delbary is supported by a post doctoral fellowship from the Villum Kann Rasmussen Foundation.

References

[1] A.P. Calderón, *On an inverse boundary value problem*, in *Seminar on Numerical Analysis and its Applications to Continuum Physics (Rio de Janeiro, 1980)* Soc. Brasil. Mat., Rio de Janeiro, 1980, pp. 65–73.
[2] D.S. Holder *Electrical Impedance Tomography: Methods, History And Applications*, Series in Medical Physics and Biomedical Engineering Institute of Physics Publishing, 2004.
[3] J. Sylvester and G. Uhlmann, *A global uniqueness theorem for an inverse boundary value problem*, Ann. of Math. (2) 125 (1987), pp. 153–169.
[4] R.M. Brown and R.H. Torres, *Uniqueness in the inverse conductivity problem for conductivities with 3/2 derivatives in L^p, $p > 2n$*, J. Fourier Anal. Appl. 9 (2003), pp. 563–574.
[5] L. Päivärinta, A. Panchenko, and G. Uhlmann, *Complex geometrical optics solutions for Lipschitz conductivities*, Rev. Mat. Iberoamericana 19 (2003), pp. 57–72.
[6] R.G. Novikov, *A multidimensional inverse spectral problem for the equation $-\Delta\psi+(v(x)-Eu(x))\psi = 0$*, Funktsional. Anal. i Prilozhen. 22 (1988), pp. 11–22, 96.
[7] A.I. Nachman, *Reconstructions from boundary measurements*, Ann. of Math. (2) 128 (1988), pp. 531–576.
[8] ———, *Global uniqueness for a two-dimensional inverse boundary value problem*, Ann. of Math. (2) 143 (1996), p. 71.
[9] S. Siltanen, J.L. Mueller, and D. Isaacson, *An implementation of the reconstruction algorithm of A. Nachman for the 2D inverse conductivity problem*, Inverse Problems 16 (2000), pp. 681–699.
[10] S. Siltanen, J. Mueller, and D. Isaacson, *Erratum: "An implementation of the reconstruction algorithm of A. Nachman for the 2D inverse conductivity problem [Inverse Problems* **16** *(2000), no. 3, 681–699; MR1766226 (2001g:35269)]*, Inverse Problems 17 (2001), pp. 1561–1563.
[11] J.L. Mueller and S. Siltanen, *Direct reconstructions of conductivities from boundary measurements*, SIAM J. Sci. Comput. 24 (2003), pp. 1232–1266.
[12] K. Knudsen, M. Lassas, J.L. Mueller, and S. Siltanen, *D-bar method for Electrical Impedance Tomography with discontinuous conductivities*, SIAM J. Appl. Math. 67 (2007), pp. 893–913.
[13] ———, *Reconstructions of piecewise constant conductivities by the D-bar method for electrical impedance tomography*, Journal of Physics: Conference Series 124 (2008), p. 012029.
[14] ———, *Regularized D-bar method for the inverse conductivity problem*, Inverse Probl. Imaging 3 (2009), pp. 599–624.
[15] J. Bikowski, K. Knudsen, and J.L. Mueller, *Direct numerical reconstruction of conductivities in three dimensions using scattering transforms*, Inverse Problems 27 (2011).
[16] K. Knudsen and J.L. Mueller, *The Born approximation and Calderón's method for reconstruction of conductivities in 3-D*, to appear.
[17] K. Astala and L. Päivärinta, *Calderón's inverse conductivity problem in the plane*, Ann. of Math. (2) 163 (2006), pp. 265–299.

[18] K. Astala, J.L. Mueller, L. Paivarinta, A. Peramaki, and S. Siltanen, *Direct electrical impedance tomography for nonsmooth conductivities*, Inverse Probl. Imaging, to appear.
[19] M. Brühl, *Explicit characterization of inclusions in electrical impedance tomography*, SIAM J. Math. Anal. 32 (2001), pp. 1327–1341 (electronic).
[20] M. Brühl and M. Hanke, *Numerical implementation of two noniterative methods for locating inclusions by impedance tomography*, Inverse Problems 16 (2000), pp. 1029–1042.
[21] A. Kirsch and N. Grinberg *The factorization method for inverse problems*, Oxford Lecture Series in Mathematics and its Applications Vol. 36, Oxford University Press, Oxford, 2008.
[22] H. Eckel and R. Kress, *Nonlinear integral equations for the inverse electrical impedance problem*, Inverse Problems 23 (2007), pp. 475–491.
[23] ———, *Non-linear integral equations for the complete electrode model in inverse impedance tomography*, Appl. Anal. 87 (2008), pp. 1267–1288.
[24] L. Borcea, *Electrical impedance tomography*, Inverse Problems 18 (2002), pp. R99–R136.
[25] H. Cornean, K. Knudsen, and S. Siltanen, *Towards a d-bar reconstruction method for three-dimensional EIT*, J. Inverse Ill-Posed Probl. 14 (2006), pp. 111–134.
[26] L.D. Faddeev, *Growing solutions to the Schrödinger equation*, Soviet Physics Dokl. 6 (1965 (transl. Sov. Phys. Dokl. 10, 1033)), pp. 514–517.
[27] M. DeAngelo and J.L. Mueller, *2D D-bar reconstructions of human chest and tank data using an improved approximation to the scattering transform*, Physiol. Meas. 31 (2010), pp. 221–232.
[28] J.L. Mueller and S. Siltanen, *Direct reconstructions of conductivities from boundary measurements*, SIAM J. Sci. Comput. 24 (2003), pp. 1232–1266.
[29] G. Boverman, T.J. Kao, D. Isaacson, and G.J. Saulnier, *An Implementation of Calderón's Method for 3-D Limited-View EIT*, IEEE Trans. Med. Imaging 28 (2009), pp. 1073–1082.
[30] R. Kress *Linear integral equations*, Second , Applied Mathematical Sciences Vol. 82, Springer-Verlag, New York, 1999.
[31] D. Colton and R. Kress *Inverse acoustic and electromagnetic scattering theory*, Second , Applied Mathematical Sciences Vol. 93, Springer-Verlag, Berlin, 1998.
[32] Boost C++ Libraries; `http://www.boost.org`.
[33] E. Anderson et al. *LAPACK Users' Guide*, Third Society for Industrial and Applied Mathematics, Philadelphia, PA, 1999.
[34] The OpenMP® API specification for parallel programming; `http://openmp.org`.
[35] Open MPI: Open Source High Performance Computing; `http://www.open-mpi.org`.
[36] L. Wienert *Die numerische Approximation von Randintegraloperatoren für die Helmholtzgleichung im* R^3, 1990, Thesis (Ph.D.)–Georg-August-Universität Göttingen.
[37] I.H. Sloan, *Polynomial interpolation and hyperinterpolation over general regions*, J. Approx. Theory 83 (1995), pp. 238–254.
[38] K. Hesse and I.H. Sloan, *Hyperinterpolation on the sphere*, in *Frontiers in interpolation and approximation* Chapman & Hall/CRC, Boca Raton, FL, 2007, pp. 213–248.